Journal of Aircraft
Vol. 46, No. 6, November–December 2009

Engineering Notes

Aeroservoelastic Analysis for Transonic Missile Based on Computational Fluid Dynamics

Weiwei Zhang,* Zhengyin Ye,† and
Chen'an Zhang‡
Northwestern Polytechnical University,
710072 Xi'an, People's Republic of China

DOI: 10.2514/1.45249

I. Introduction

AEROELASTICITY is a multidisciplinary field of study dealing with the interaction of inertia, structural, and aerodynamic forces. Flutter is a typical aeroelastic problem that can cause an unstable vibration. With the improvement of electrical technique, many kinds of flight control systems are widely used in new aircraft. The new problem is joined with aerodynamics, elasticity, and control systems, and designers should check the stability of the problem of aeroservoelasticity. In the transonic flow region, the shock position is very sensitive to structural vibration, and there is an obvious delay between structural motion and the aerodynamic force. A dip often appears on the flutter boundary in the transonic region, and it often leads to a bottleneck problem in the flight envelope.

Some simple models are still used [1] to calculate the aerodynamic loads of missiles in the aircraft design institute (e.g., slender-body theory for the body and strip theory for the wings). Most of those classical methods are difficult to use when considering the interference between the wing and the body. Lifting surface methods based on linear theory have also been used for unsteady aerodynamic computation and flutter analysis [2], such as the doublet lattice aerodynamic model in NASTRAN [3]. This kind of method needs to compute the generalized aerodynamic force for a range of frequencies for each structural mode. Nevertheless, this method is confined to planforms of very thin sections at small angles of attack, whereby neither thickness effect nor angles of attack can be accounted for; it is also incapable in transonic flow.

For the transonic flutter problems, it is important to simulate the nonlinear unsteady aerodynamics with the presence of shock movements. With the progress in CPU speeds, computational fluid dynamics (CFD)-based time-integration techniques have been used in aircraft design [4,5]. Coupling structural equations with an Euler/Navier–Stokes-based unsteady CFD algorithm, the structural aeroelastic responses can be predicted in the time domain. Those methods are suitable for solving the nonlinear transonic flutter problems, because they make the fewest assumptions about the characteristics of the flows. However, the challenge of these kinds of methods is their ineffective use in the preliminary aeroelastic design stage.

Recently, much research was carried out in reduced order modeling (ROM) for unsteady aerodynamics. It is novel, in that it captures (to some extent) the nonlinear flow characteristics, and it is more computationally efficient than full-CFD simulation. It is very suitable for predicting the flutter boundary in transonic flow. There are two kinds of methods to construct the reduced-order aerodynamic models. One is the proper orthogonal decomposition (POD) technique [6–10], and the other is aerodynamic modeling based on the system identification technique [11–22].

POD is a method that is used extensively at several research organizations for the development of ROMs. A thorough review of POD research activities can be found in the paper by Lucia et al. [6]. Romanowski [7] is perhaps the first to introduce the POD technique to construct the reduced-order aerodynamic model for flutter analysis. In addition, a review of the issues involved in the development of ROMs for aeroelastic problems is provided by Dowell and Hall [9]. A topic of recent interest is the potential development of parameter adaptation of the reduced order models at different Mach numbers; two interpolation methods for adapting the POD basis vectors to varying Mach numbers are presented in [10].

A simplified aerodynamic model that captures the dominant dynamics of the flow can also be constructed by the system identification technique. Silva [11] is among the first to introduce nonlinear Volterra theory to unsteady aerodynamics. Based on unit impulse responses, the first-order (linear) kernel and the second-order (nonlinear) kernel are numerically identified for a single-input–single-output system. Silva and Bartels [12], Marzocca et al. [13], and Raveh [14] have also applied the Volterra kernel identification technique into aeroelastic systems. The Volterra kernels are approximated in terms of orthonormal piecewise-polynomial multiwavelets. A least square (LS) problem is solved for the multiwavelet coefficients that represent the kernels. As for the second- and higher-order kernels, a very large number of coefficients are required for accuracy. Raveh [15] found that when the nonlinear system is assumed to be a second-order system, the convolved response (based on the Volterra ROM) was extremely sensitive to the amplitude of the impulse inputs used for kernel identification. Only when the step amplitude was closer to that of the direct excitation signal was the prediction accuracy improved. Assuming the system to be a second order did not improve the ROM when compared with a first-order ROM.

Cowan et al. [16] used a kind of input–output difference model [autoregressive with exogenous input model (ARX)] to represent the relationship between generalized aerodynamic force coefficients and structural modal coordinates. A multiple-step input signal is used to prescribe the motion of the modal, and then CFD solutions are carried out to provide a complete data set (input/output) for training. Once the model is defined, it is used in place of the CFD codes in the coupled structural equations to predict the structural responses. Raveh [17] used two types of input signals for modal coordinates: one is the random time series and the other is a filtered random series with Gaussian distribution for system identification of unsteady aerodynamics. Three types of modeling between the generalized aerodynamic force coefficients (outputs) and modal coordinates (inputs) are constructed: a frequency domain model, a discrete-time-domain model, and a discrete-time-domain state-space model. The efficiency of this kind of ROM-based method is improved up to $1 \sim 2$

Presented as Paper 6482 at the AIAA Modeling and Simulation Technologies Conference and Exhibit, Hilton Head, SC, 20–23 August 2007; received 3 May 2009; revision received 29 August 2009; accepted for publication 9 September 2009.

*Associate Professor, National Key Laboratory of Aerodynamic Design and Research, College of Aeronautics; zww12345@sina.com. Member AIAA. (Corresponding author).
†Professor, National Key Laboratory of Aerodynamic Design and Research, College of Aeronautics; yezy@nwpu.edu.cn.
‡Ph.D. Student, National Key Laboratory of Aerodynamic Design and Research, College of Aeronautics; zhch_a@163.com.

orders by comparing it with the direct CFD simulation method [16,18].

In this paper, the ROM is developed by using the system identification technique similar to that of Cowan et al. [16] and Raveh [17], but the discrete-time-domain state-space model is transferred to a continuous time-domain state-space model. This kind of ROM has been used to perform flutter studies at a high angle of attack [19] and gust response analysis [20] and transonic flutter suppression by active control [21]. Marzocca et al. [13] and Stephens et al. [22] employed ROM to a closed-loop aeroelastic study. Coupling the open-loop aeroelastic system with a given control law, the closed-loop aeroelastic responses were solved using time-integration techniques. However, this kind of simulation method is still not suitable for parametric studies and qualitative analysis in the preliminary design stage. In the present paper, ROM is used to build a model for aeroservoelastic analysis in state space and to study the aeroservoelastic characteristics of a transonic missile.

II. Methodology

A. Transonic Unsteady Aerodynamic Models

A high-quality unsteady aerodynamic model is the base of aeroelastic studies. An Euler-equations-based unsteady flow solver has the ability to simulate the flow with strong shock and shock motion, which is used in the following studies. It is more efficient and more mature when compared with the N–S-equations-based flow solvers. The Euler-equations-based solver is based on unstructured mesh because of its convenience for complex configurations, such as a wing-body configuration. Spatial discretization is accomplished by the cell-centered finite volume method using a center scheme. A second-order-accurate full-implicit scheme is used to integrate the equations in time, and the fourth Runge–Kutta method is used in the pseudotime stepping. A more detailed process can be found in [18].

An identification technique is used to construct the reduced-order model based on the structural modes. The time cost of the ROM-based flutter analysis method is mainly used in training the model. Because the unsteady loads are computed in a discrete domain, the ARX model is chosen for the multi-input–multi-output system, which is shown in Eq. (1):

$$\boldsymbol{f}_a(k) = \sum_{i=1}^{na} \boldsymbol{A}_i \boldsymbol{f}_a(k-i) + \sum_{i=0}^{nb-1} \boldsymbol{B}_i \boldsymbol{\xi}(k-i) \tag{1}$$

where $\boldsymbol{f}_a$ is the vector of system outputs (generalized aerodynamic force coefficient vector) and $\boldsymbol{\xi}$ is the vector of system inputs (generalized structural mode coordinate vector). $\boldsymbol{A}_i$ and $\boldsymbol{B}_i$ are the constant coefficients to be estimated. The model orders determined by the user are na and nb. Multistep input is employed due to its easy of implementation and broad frequency content. The LS method is used to estimate the unknown model parameters. To make the data have a zero mean, the data need to remove the constant levels before they are estimated.

To derive the state-space form for aeroelastic analysis, we define a state vector $\boldsymbol{x}_a(k)$ consisting of $(na + nb - 1)$ vector states as follows:

$$\boldsymbol{x}_a(k) = [\boldsymbol{f}_a(k-1), \cdots, \boldsymbol{f}_a(k-na), \boldsymbol{\xi}(k-1), \ldots, \boldsymbol{\xi}(k-nb+1)]^T \tag{2}$$

The state-space form for the discrete-time aerodynamic model is as follows:

$$\begin{cases} \boldsymbol{x}_a(k+1) = \tilde{\boldsymbol{A}}_a \boldsymbol{x}_a(k) + \tilde{\boldsymbol{B}}_a \boldsymbol{\xi}(k) \\ \boldsymbol{f}_a(k) = \tilde{\boldsymbol{C}}_a \boldsymbol{x}_a(k) + \tilde{\boldsymbol{D}}_a \boldsymbol{\xi}(k) \end{cases} \tag{3}$$

where

$$\tilde{\boldsymbol{A}}_a = \begin{bmatrix} \boldsymbol{A}_1 & \boldsymbol{A}_2 & \cdots & \boldsymbol{A}_{na-1} & \boldsymbol{A}_{na} & \boldsymbol{B}_1 & \boldsymbol{B}_2 & \cdots & \boldsymbol{B}_{nb-2} & \boldsymbol{B}_{nb-1} \\ \boldsymbol{I} & \boldsymbol{0} & \cdots & \boldsymbol{0} & \boldsymbol{0} & \boldsymbol{0} & \boldsymbol{0} & \cdots & \boldsymbol{0} & \boldsymbol{0} \\ \vdots & \boldsymbol{I} & \cdots & \boldsymbol{0} & \boldsymbol{0} & \boldsymbol{0} & \boldsymbol{0} & \cdots & \boldsymbol{0} & \boldsymbol{0} \\ \vdots & \vdots & \ddots & \vdots & \vdots & \vdots & \vdots & \ddots & \vdots & \vdots \\ \boldsymbol{0} & \boldsymbol{0} & \cdots & \boldsymbol{I} & \boldsymbol{0} & \boldsymbol{0} & \boldsymbol{0} & \cdots & \boldsymbol{0} & \boldsymbol{0} \\ \boldsymbol{0} & \boldsymbol{0} & \cdots & \boldsymbol{0} & \boldsymbol{0} & \boldsymbol{0} & \boldsymbol{0} & \cdots & \boldsymbol{0} & \boldsymbol{0} \\ \boldsymbol{0} & \boldsymbol{0} & \cdots & \boldsymbol{0} & \boldsymbol{0} & \boldsymbol{I} & \boldsymbol{0} & \cdots & \boldsymbol{0} & \boldsymbol{0} \\ \boldsymbol{0} & \boldsymbol{0} & \cdots & \boldsymbol{0} & \boldsymbol{0} & \boldsymbol{0} & \boldsymbol{I} & \cdots & \boldsymbol{0} & \boldsymbol{0} \\ \vdots & \vdots & \ddots & \vdots & \vdots & \vdots & \vdots & \ddots & \vdots & \vdots \\ \boldsymbol{0} & \boldsymbol{0} & \cdots & \boldsymbol{0} & \boldsymbol{0} & \boldsymbol{0} & \boldsymbol{0} & \cdots & \boldsymbol{I} & \boldsymbol{0} \end{bmatrix}$$

$$\tilde{\boldsymbol{B}}_a = [\tilde{\boldsymbol{B}}_0 \quad \boldsymbol{0} \quad \boldsymbol{0} \quad \cdots \quad \boldsymbol{0} \quad \boldsymbol{I} \quad \boldsymbol{0} \quad \boldsymbol{0} \quad \cdots \quad \boldsymbol{0}]^T$$

$$\tilde{\boldsymbol{C}}_a = [\boldsymbol{A}_1 \quad \boldsymbol{A}_2 \quad \cdots \quad \boldsymbol{A}_{na-1} \quad \boldsymbol{A}_{na} \quad \boldsymbol{B}_1 \quad \boldsymbol{B}_2 \quad \cdots \quad \boldsymbol{B}_{nb-2} \quad \boldsymbol{B}_{nb-1}]$$

$$\tilde{\boldsymbol{D}}_a = [\boldsymbol{B}_0]$$

To couple the structural equations, the discrete-time state-space form is turned into the continue-time form, and the model in state-space form is constructed as shown in Eq. (4):

$$\begin{cases} \dot{\boldsymbol{x}}_a(t) = \boldsymbol{A}_a \boldsymbol{x}_a(t) + \boldsymbol{B}_a \boldsymbol{\xi}(t) \\ \boldsymbol{f}_a(t) = \boldsymbol{C}_a \boldsymbol{x}_a(t) + \boldsymbol{D}_a \boldsymbol{\xi}(t) \end{cases} \tag{4}$$

A more detailed process can be found in [18,19].

B. Open-Loop Aeroelastic Model

Equation (5) is the structural equation of motion:

$$\boldsymbol{M} \cdot \ddot{\boldsymbol{\xi}} + \boldsymbol{G} \cdot \dot{\boldsymbol{\xi}} + \boldsymbol{K} \cdot \boldsymbol{\xi} = \boldsymbol{F} = q.\boldsymbol{f}_a \tag{5}$$

$\boldsymbol{M}$, $\boldsymbol{K}$, $\boldsymbol{F}$, and q are the mass matrix, stiffness matrix, generalized forces vector, and free stream dynamic pressure.

Defining the structural state vector $\boldsymbol{x}_s = [\boldsymbol{\xi}, \dot{\boldsymbol{\xi}}]^T$, the structural equations in state-space form would be

$$\begin{cases} \dot{\boldsymbol{x}}_s(t) = \boldsymbol{A}_s \cdot \boldsymbol{x}_s(t) + q \cdot \boldsymbol{B}_s \cdot \boldsymbol{f}_a(t) \\ \boldsymbol{\xi}(t) = \boldsymbol{C}_s \cdot \boldsymbol{x}_s(t) + q.\boldsymbol{D}_s \cdot \boldsymbol{f}_a(t) \end{cases} \tag{6}$$

where

$$\boldsymbol{A}_s = \begin{bmatrix} \boldsymbol{O} & \boldsymbol{I} \\ -\boldsymbol{M}^{-1}\boldsymbol{K} & -\boldsymbol{M}^{-1}\boldsymbol{G} \end{bmatrix}, \qquad \boldsymbol{B}_s = \begin{bmatrix} \boldsymbol{O} \\ \boldsymbol{M}^{-1} \end{bmatrix}$$

$$\boldsymbol{C}_s = [\boldsymbol{I} \quad \boldsymbol{0}], \qquad \boldsymbol{D}_s = [\boldsymbol{0}]$$

By defining the open-loop state vector $\boldsymbol{x}_{\mathrm{as}} = [\boldsymbol{x}_s, \boldsymbol{x}_a]^T$ and coupling the structural state equations (6) with aerodynamic state equations (4), we get state equations and output equations for the open-loop aeroelastic system as follows (with the subscript of as):

$$\begin{cases} \dot{\boldsymbol{x}}_{\mathrm{as}}(t) = \boldsymbol{A}_{\mathrm{as}} \cdot \boldsymbol{x}_{\mathrm{as}}(t) + \boldsymbol{B}_{\mathrm{as}} \cdot \boldsymbol{F}(t) \\ \boldsymbol{y}_{\mathrm{as}}(t) = [\omega_y, a_z]^T = \boldsymbol{E} \cdot \dot{\boldsymbol{x}}_s(t) = \boldsymbol{C}_{\mathrm{as}} \cdot \boldsymbol{x}_{\mathrm{as}}(t) + \boldsymbol{D}_{\mathrm{as}} \cdot \boldsymbol{F}(t) \end{cases} \tag{7}$$

where

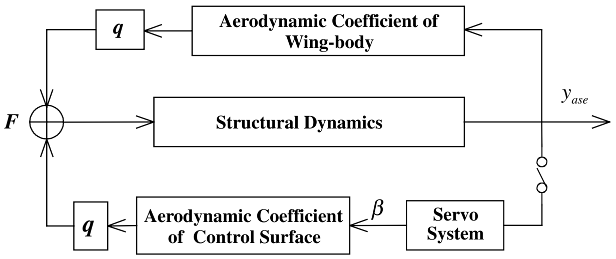

Fig. 1 Block diagram of aeroservoelasticity.

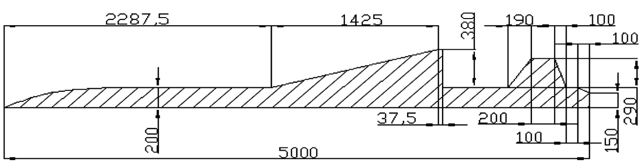

Fig. 2 Computational model.

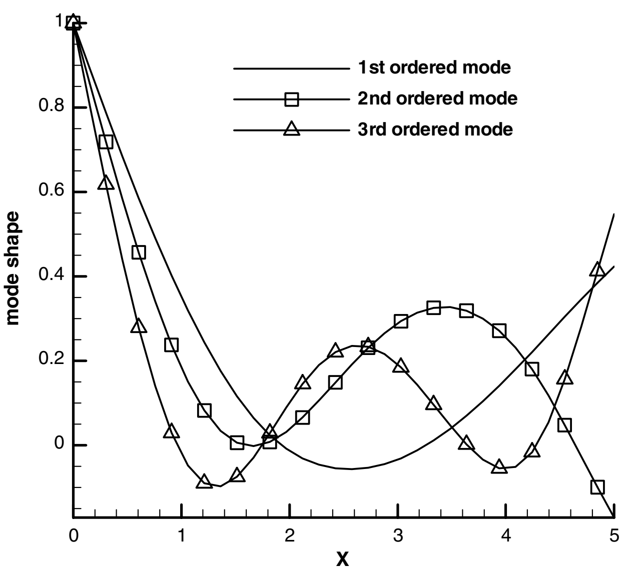

Fig. 3 The first, second, and third mode shapes of the body.

$$\boldsymbol{A}_{\mathrm{as}} = \begin{bmatrix} \boldsymbol{A}_s + q \cdot \boldsymbol{B}_s \boldsymbol{D}_a \boldsymbol{C}_s & q \cdot \boldsymbol{B}_s \boldsymbol{C}a \\ \boldsymbol{B}_a \boldsymbol{C}_s & \boldsymbol{A}_a \end{bmatrix}, \qquad \boldsymbol{B}_{\mathrm{as}} = \begin{bmatrix} \boldsymbol{B}_s \\ \boldsymbol{0} \end{bmatrix}$$

$$\boldsymbol{C}_{\mathrm{as}} = \boldsymbol{E} \cdot [\boldsymbol{C}_S, \boldsymbol{0}] \cdot \boldsymbol{A}_{\mathrm{as}}, \qquad \boldsymbol{D}_{\mathrm{as}} = \boldsymbol{E} \cdot [\boldsymbol{C}_S, \boldsymbol{0}] \cdot \boldsymbol{B}_{\mathrm{as}}$$

$$\boldsymbol{E} = \begin{bmatrix} \partial z x_1/\partial z, \ \cdots, \ \partial z x_n/\partial z, 0_{n\times 1} \\ 0_{n\times 1}, \ z x_1, \ \cdots, \ z x_n \end{bmatrix}$$

w_y and a_z are the pitching rate and the normal acceleration at the position of the sensor, zx_i is the mode shape at the place of the sensor, and n is the number of the chosen structural modes.

Table 1 Structural frequencies of the missile

	Body			Wing			Control surface		
Mode	1	3	6	4	7	9	2	5	8
Freq., rad/s	70	200	400	250	500	850	125	325	660

Table 2 Open-loop results comparison between ROM-based analysis and Euler-based simulation at the flutter state ($M = 0.9$)

	$V_f/\mathrm{m \cdot s^{-1}}$	$\omega_f/\mathrm{rad \cdot s^{-1}}$	Proportion of amplitude (A_1/A_2)	$(\varphi_1 - \varphi_2)/$ deg
ROM	312.0	70.2	0.284	163.23
Euler	315	69.0	0.25	163.25
Error	0.96%	1.2%	0.034	0.012%

C. Closed-Loop Aeroelastic Model

After constructing the open-loop aeroelastic model, the closed-loop model can be constructed by combining an open-loop aeroelastic system, a servo system, and the aerodynamic system of the control surface (as shown in Fig. 1).

Considering the position of the sensor, the dynamic characteristics of the sensor, and the rudder, the servo control system can be defined in state space as follows (with the subscript of c):

$$\begin{cases} \dot{\boldsymbol{x}}_c(t) = \boldsymbol{A}_c \boldsymbol{x}_c(t) + \boldsymbol{B}_c \boldsymbol{y}_{\mathrm{as}}(t) \\ \beta(t) = \boldsymbol{C}_c \boldsymbol{x}_c(t) + \boldsymbol{D}_c \boldsymbol{y}_{\mathrm{as}}(t) \end{cases} \tag{8}$$

where β is the angle of flap displacement (down deflection is positive), $\boldsymbol{D}_c$ is always a zero matrix.

An open-loop aeroelastic system [Eq. (7)] and a servo system [Eq. (8)] are then combined in series. Defining $\boldsymbol{x}_{\mathrm{as}c} = [\boldsymbol{x}_{\mathrm{as}}, \boldsymbol{x}_c]^T$, we get

$$\begin{cases} \dot{\boldsymbol{x}}_{\mathrm{as}c}(t) = \boldsymbol{A}_{\mathrm{as}c} \boldsymbol{x}_{\mathrm{as}c}(t) + \boldsymbol{B}_{\mathrm{as}c} \boldsymbol{F} \\ \beta(t) = \boldsymbol{C}_{\mathrm{as}c} \boldsymbol{x}_{\mathrm{as}c}(t) + \boldsymbol{D}_{\mathrm{as}c} \boldsymbol{F} \end{cases} \tag{9}$$

where

$$\boldsymbol{A}_{\mathrm{as}c} = \begin{bmatrix} \boldsymbol{A}_{\mathrm{as}} & \boldsymbol{0} \\ \boldsymbol{B}_c \boldsymbol{C}_{\mathrm{as}} & \boldsymbol{A}_c \end{bmatrix}, \qquad \boldsymbol{B}_{\mathrm{as}c} = \begin{bmatrix} \boldsymbol{B}_{\mathrm{as}} \\ \boldsymbol{B}_c \boldsymbol{D}_{\mathrm{as}} \end{bmatrix}$$

$$\boldsymbol{C}_{\mathrm{as}c} = [\boldsymbol{0}, \boldsymbol{C}_c], \qquad \boldsymbol{D}_{\mathrm{as}c} = [\boldsymbol{0}]$$

For the closed-loop aeroelastic problem, feedback control is carried out by the additional aerodynamics produced by the active motion of the control surface. The aerodynamic state-space equations of the control surface can be modeled as the same as that of Eq. (4). It is shown as follows (with the subscript of ac):

$$\begin{cases} \dot{\boldsymbol{x}}_{\mathrm{ac}}(t) = \boldsymbol{A}_{\mathrm{ac}} \boldsymbol{x}_{\mathrm{ac}}(t) + \boldsymbol{B}_{\mathrm{ac}} \beta(t) \\ \boldsymbol{F} = q \cdot \boldsymbol{f}_{\mathrm{ac}}(t) = q \cdot \boldsymbol{C}_{\mathrm{ac}} \boldsymbol{x}_{\mathrm{ac}}(t) + q \cdot \boldsymbol{D}_{\mathrm{ac}} \beta(t) \end{cases} \tag{10}$$

where $\boldsymbol{f}_{\mathrm{ac}}$ is the additional aerodynamic coefficient vector of the control surface.

By defining $\boldsymbol{x}_{\mathrm{as}e} = [\boldsymbol{x}_{\mathrm{as}c}, \boldsymbol{x}_{\mathrm{ac}}]^T$, we can combine the subsystem [which is defined by Eq. (9)] and the aerodynamic system of the control surface [which defined by Eq. (10)] in feedback style and

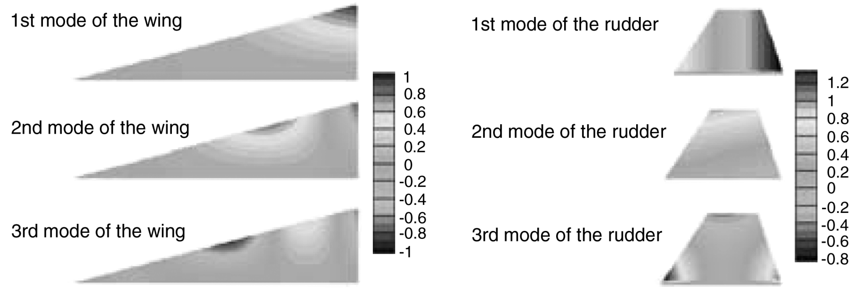

Fig. 4 The first, second, and third mode shapes of the wing and the rudder.

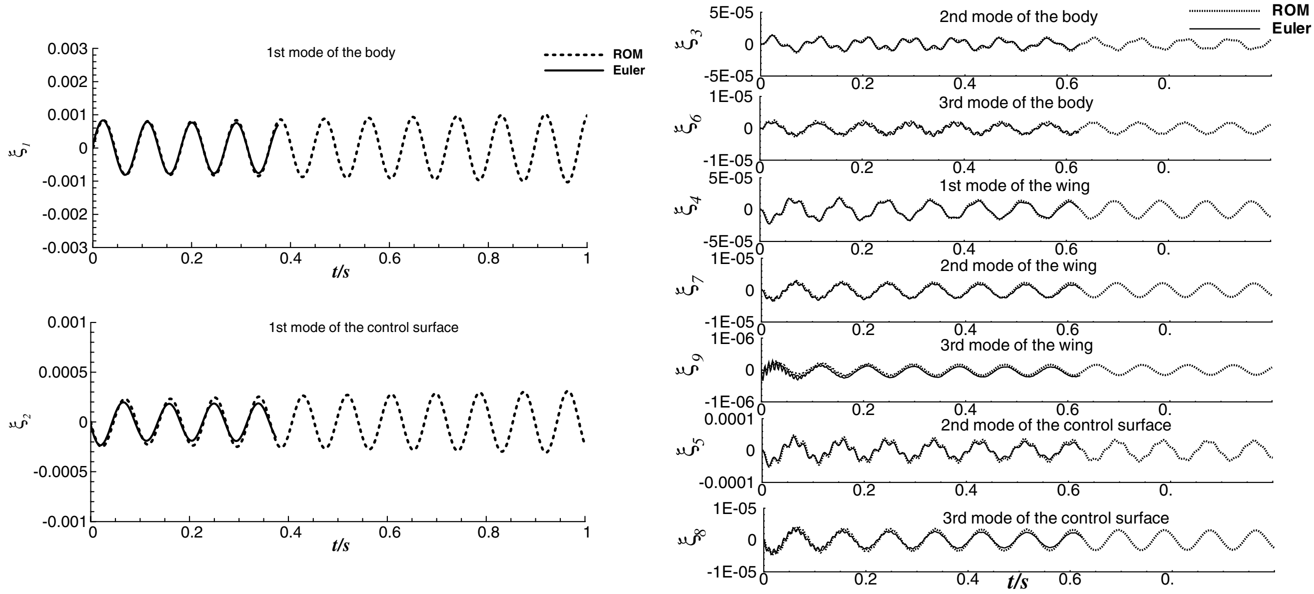

a) The time history of the main flutter branches

b) The time history of the other branches

Fig. 5 The time history of the open-loop missile system ($M = 0.9$, $v = 315$ m/s).

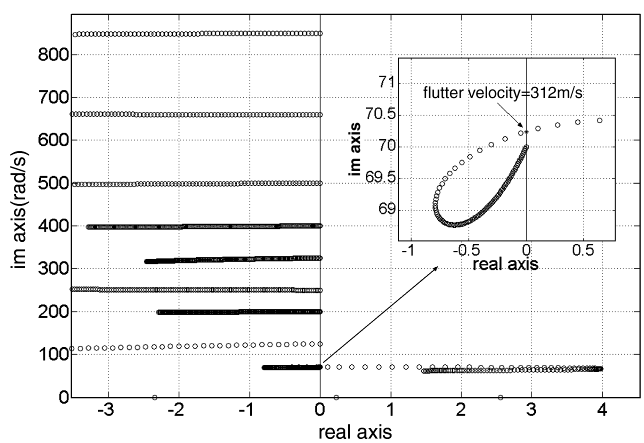

Fig. 6 Root loci of the open-loop aeroelastic system ($M = 0.9$).

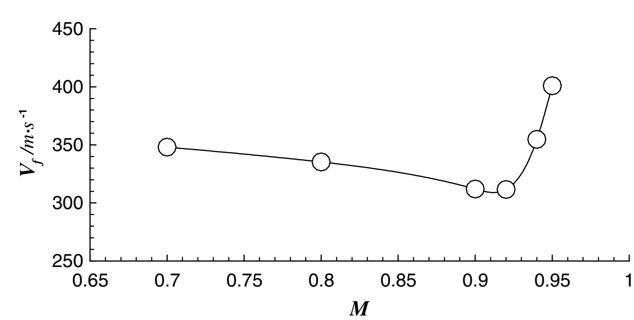

Fig. 7 The variation of flutter speed with Mach number.

get the aeroservoelastic equations in state space (with the subscript of ase):

$$\dot{\boldsymbol{x}}_{\mathrm{ase}} = \boldsymbol{A}_{\mathrm{ase}} \cdot \boldsymbol{x}_{\mathrm{ase}} = \begin{bmatrix} \boldsymbol{A}_{\mathrm{asc}} + q \cdot \boldsymbol{B}_{\mathrm{asc}} \cdot \boldsymbol{D}_{\mathrm{ac}} \cdot \boldsymbol{C}_{\mathrm{asc}} & q \cdot \boldsymbol{B}_{\mathrm{asc}} \cdot \boldsymbol{C}_{\mathrm{ac}} \\ \boldsymbol{B}_{\mathrm{ac}} \cdot \boldsymbol{C}_{\mathrm{asc}} & \boldsymbol{A}_{\mathrm{ac}} \end{bmatrix} \cdot \boldsymbol{x}_{\mathrm{ase}} \tag{11}$$

Analysis of the transonic aeroservoelastic characteristics is then turned into the solution of a complex eigenvalue problem of matrix $\boldsymbol{A}_{\mathrm{ase}}$.

III. Results and Analysis

For the transonic aeroservoelastic problem, few experimental or standard numerical models with detailed parameters can be found. In this paper, a missile with a typical double crosses layout wing (++) is designed, which can be seen from Fig. 2. The control surface is a completely active rudder. Figures 3 and 4 show the mode shapes of the body, wing, and rudder. Table 1 shows the mode frequencies of the missile.

Table 2 and Fig. 5 show the compared open-loop aeroelastic results. The computational states are $M = 0.9$, $\alpha = 0$ deg, and $\rho = 1.0$ kg/m^3. We can find that flutter results calculated by a ROM-based method agree well with those by a CFD direct simulation method. Figure 6 shows root loci of the open-loop aeroelastic system. We can find that the instability of the missile at this state is caused mostly by the coupling effects of the body's first mode and the rudder's first mode. Figure 7 shows the flutter boundary of the missile in a transonic region. It can be found that a dip appears on the curve near Mach number 0.92.

A typical closed-loop control law is designed for the missile. The pitching rate sensor is used in the control system. Table 3 and Fig. 8 show the effects of the sensor positions on the aeroservoelastic system (x_s represents the distance between the sensor and the tip of the missile). Because the first mode of the body is one of the main flutter branches, Table 3 shows the slope of the first mode of the body k_1 which relates to the pitching rate sensor. The closed-loop without a structural filter greatly changes the aeroelastic characteristics of the missile. When $k_1 < 0$, the closed-loop reduces the flutter speed; the smaller the absolute value of k_1, the lower the flutter speed is. When the sensor is placed at the tip of the missile, there is a reduction to 20%

Table 3 Characteristics of an aeroservoelastic system for different positions of the sensor

Positions of sensor, x_s/m	Slope of the first mode, k_1	V_f/m · s^{-1} Without filter	With filter
0.61	−0.729	255.3	311.8
1.06	−0.594	262.3	311.9
1.82	−0.251	285.1	311.9
2.27	−0.073	302.5	312.0
3.03	0.125	No flutter	312.0
3.48	0.221	Instability at low speed	312.0
4.09	0.300		312.0

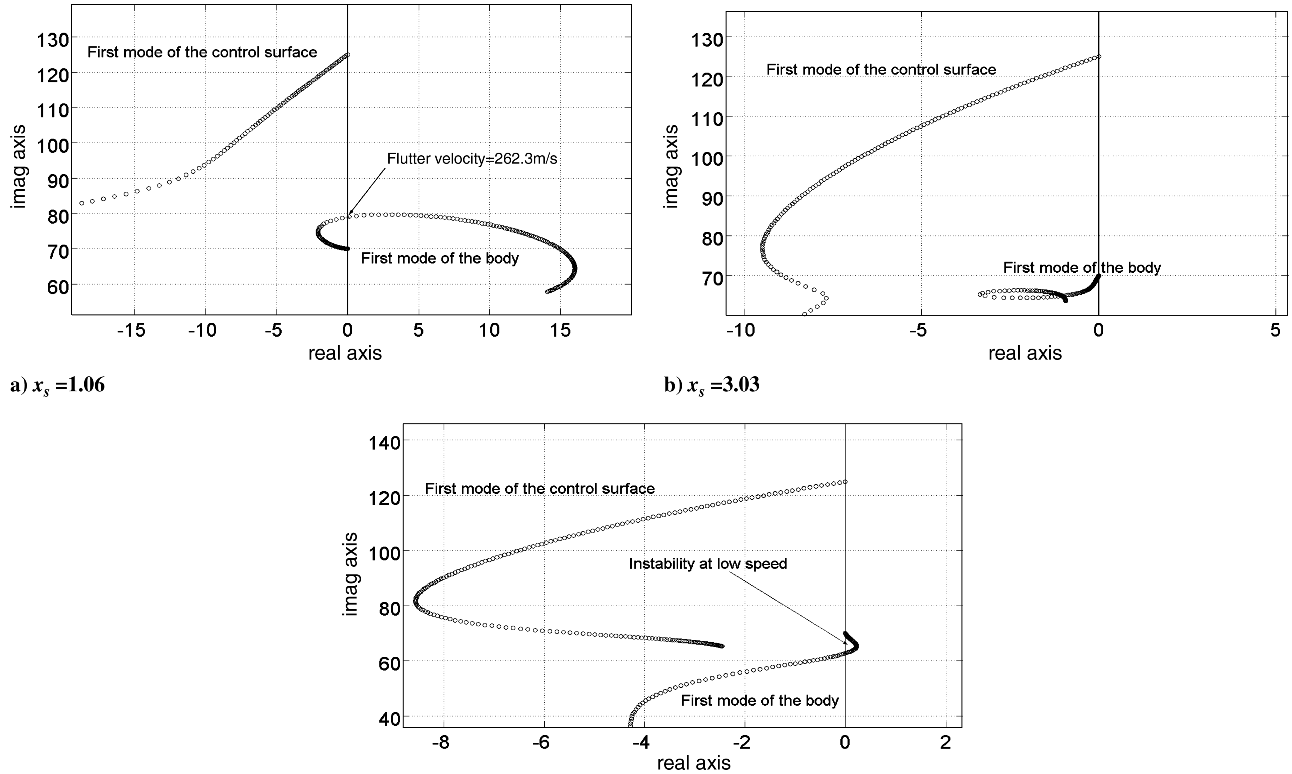

a) x_s **=1.06** **b)** x_s **=3.03** **c)** x_s **=3.48**

Fig. 8 Root loci of the closed-loop system for the different positions of the sensor.

on the flutter speed when comparing with the open-loop results. When the sensor is placed at the zero slope of the mode shape, the servo system has minimum effect on the flutter characteristics. When $k_1 < 0$ and ($x_s > 2.5$ m), the closed-loop flutter characteristics of the missile change thoroughly. When $x_s = 3.03$ m, flutter will not appear, as shown in Fig. 8b. When the sensor is moved back, instability appears at a low speed. The real parts of the eigenvalues at the right quadrants are very small (Fig. 8c), and so the flutter grows slowly.

A structural filter for 70 rad/s is then added in the closed loop. Figure 9 shows the body diagram of the control system. From the computational results in Table 3, we can see the addition of a structural filter can reduce the coupling effect between the open-loop aeroelastic system and the active control system greatly. The

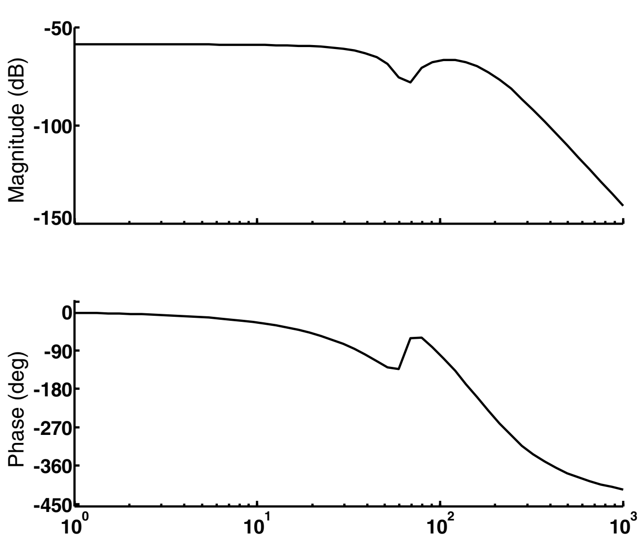

Fig. 9 Body diagram of the control system.

characteristics of the closed-loop aeroelasticity with structural filter are almost the same as those of the open-loop problem.

IV. Conclusions

By using CFD technology and the system identification method, the transonic unsteady aerodynamic model is constructed first. Combining aerodynamic state equations, structural equations, and servo equations, the closed-loop aeroelastic models for the transonic missile are constructed. The results analyzed by the ROM-based method in state space are compared with those by the CFD-based direct simulation method. The good agreement shows the quality of the ROM-based method is acceptable. The numerical examples show that the present method has the following points worth mentioning.

1) High accuracy for not only the responses of time history, but also the flutter results given by ROM-based method agree well with those by the CFD-based direct simulation method. Therefore, the ROM-based method almost has the same accuracy as the CFD-based direct simulation method.

2) The method has high efficiency. In the process of aeroservoelastic analysis, only one ROM of the aerodynamics is needed for one flow state (Mach number and angle of attack). Therefore, for the different dynamic pressures, different structural frequencies, and different servo systems, it is not necessary to compute the unsteady flow repetitively, which costs most of the computational time.

3) A unification of qualitative analysis and a quantitative computation for transonic aeroelasticity is achieved. The present method, based on ROM technology in state space, not only shows the neutral flutter results, but it also provides the global aeroelastic characteristics (from which more information can be retrieved). It is more suitable for aeroservoelastic analysis and design.

The present numerical examples show that the position of the sensor greatly affects the aeroservoelastic characteristics for the servo system without a structural filter. When a structural filter is added into the closed-loop system, the aeroservoelastic characteristics of this missile are almost same as those of the open-loop system.

Acknowledgments

This work was supported by the National Natural Science Foundation (10802063), the Natural Science Foundation of the Shaanxi Province (2007A22), the Doctoral Foundation of Ministry of the Education of China (20070699065), the Creation Foundation of Northwestern Polytechnical University, and the Foundation of the National Key Laboratory of Aerodynamic Design and Research (9140C42020207ZS51). The authors would also like to thank Lingcheng Zhao and Yongnian Yang.

References

[1] Chae, S., and Hodges, D. H., "Dynamics and Aeroelastic Analysis of Missiles," AIAA Paper 2003-1968, 2003.

[2] Heinze, S., Ringertz, U., and Borglund, D., "Assessment of Uncertain External Store Aerodynamics Using μ-p Flutter Analysis," *Journal of Aircraft*, Vol. 46, No. 3, 2009, pp. 1062–1067. doi:10.2514/1.39158

[3] NASTRAN, Software Package, Ver. 2005, MSC Software Corp., Santa Ana, CA, 2005.

[4] Bendiksen, O., "High-Altitude Limit Cycle Flutter of Transonic Wings," *Journal of Aircraft*, Vol. 46, No. 1, 2009, pp. 123–136. doi:10.2514/1.36413

[5] Liu, F., Cai, J., Zhu, Y., Wong, A. S. F., and Tsai, H. M., "Calculation of Wing Flutter by a Coupled Fluid-Structure Method," *Journal of Aircraft*, Vol. 38, No. 2, 2001, pp. 334–342. doi:10.2514/2.2766

[6] Lucia, D. J., Beran, P. S., and Silva, W. A., "Reduced-Order Modeling: New Approaches for Computational Physics," *Progress in Aerospace Sciences*, Vol. 40, No. 1, 2004, pp. 51–117. doi:10.1016/j.paerosci.2003.12.001

[7] Romanowski, M. C., "Reduced Order Unsteady Aerodynamic and Aeroelastic Models Using Karunen–Loeve Eigenmodes," AIAA Paper 96-3981, 1996.

[8] Hall, K. C., Thomas, J. P., and Dowell, E. H., "Reduced-Order Modeling of Unsteady Small-Disturbance Flows Using a Frequency-Domain Proper Orthogonal Decomposition Technique," AIAA Paper 99-0655, 1999.

[9] Dowell, E. H., and Hall, K. C., "Modeling of Fluid-Structure Interaction," *Annual Review of Fluid Mechanics*, Vol. 33, Jan. 2001, pp. 445–490. doi:10.1146/annurev.fluid.33.1.445

[10] Lieu, T., and Lesoinne, M., "Parameter Adaptation of Reduced Order Models for Three-Dimensional Flutter Analysis," AIAA Paper 2004-888, 2004.

[11] Silva, W. A., "Application of Nonlinear Systems Theory to Transonic Unsteady Aerodynamic Responses," *Journal of Aircraft*, Vol. 30, No. 5, 1993, pp. 660–668. doi:10.2514/3.46395

[12] Silva, W. A., and Bartels, R. E., "Development of Reduced-Order Models for Aeroelastic Analysis and Flutter Prediction Using the CFL3Dv6.0 Code," *Journal of Fluids and Structures*, Vol. 19, No. 6, 2004, pp. 729–745. doi:10.1016/j.jfluidstructs.2004.03.004

[13] Marzocca, P., Silva, W. A., and Librescu, L., "Open/Closed-Loop Nonlinear Aeroelasticity for Airfoils Via Volterra Series Approach," *AIAA Journal*, Vol. 42, No. 4, 2004, pp. 673–686. doi:10.2514/1.9552

[14] Raveh, D. E., "Computational-Fluid-Dynamics-Based Aeroelastic Analysis and Structural Design Optimization: A Researcher's Perspective," *Computer Methods in Applied Mechanics and Engineering*, Vol. 194, Nos. 30–33, 2005, pp. 3453–3471. doi:10.1016/j.cma.2004.12.027

[15] Raveh, D. E., "Reduced-Order Models for Nonlinear Unsteady Aerodynamics," *AIAA Journal*, Vol. 39, No. 8, 2001, pp. 1417–1429. doi:10.2514/2.1473

[16] Cowan, T. J., Andrew, S. A. J., and Gupta, K. K., "Accelerating Computational Fluid Dynamics Based Aeroelastic Predictions Using System Identification," *Journal of Aircraft*, Vol. 38, No. 1, 2001, pp. 81–87. doi:10.2514/2.2737

[17] Raveh, D. E., "Identification of CFD-Based Unsteady Aerodynamic Models for Aeroelastic Analysis," 44th AIAA/ASME/ASCE/AHS Structures, Structural Dynamics, and Materials Conference, AIAA Paper 2003-1407, 2003.

[18] Zhang, W., "Efficient Analysis for Aeroelasticity Based on CFD," Ph.D. Dissertation, Northwestern Polytechnical Univ., Xi'an, PRC, 2006.

[19] Zhang, W., and Ye, Z., "Reduced-Order-Model-Based Flutter Analysis at High Angle of Attack," *Journal of Aircraft*, Vol. 44, No. 6, Nov.–Dec. 2007, pp. 2086–2089. doi:10.2514/1.32285

[20] Zhang, W., Ye, Z., Yang, Q., and Shi, A., "Gust Response Analysis Using CFD-Based Reduced Order Models," 47th AIAA Aerospace Sciences Meeting Including The New Horizons Forum and Aerospace Exposition, AIAA Paper 2009-895, Jan. 2009.

[21] Zhang, W., and Ye, Z., "Control Law Design for Transonic Aeroservoelasticity," *Aerospace Science and Technology*, Vol. 11, Nos. 2–3, 2007, pp. 136–145. doi:10.1016/j.ast.2006.12.004

[22] Stephens, C., Arena, A., and Gupta, K., "CFD Based Aeroservoelastic Predictions with Comparisons to Benchmark Experimental Data," AIAA Paper 99-0766, 1999.